

# The Growth of Red Sequence Galaxies in a Cosmological Hydrodynamic Simulation

J. M. Gabor,<sup>1,2\*</sup> R. Davé<sup>2</sup>

<sup>1</sup>CEA-Saclay, IRFU, SAp, F-91191 Gif-sur-Yvette, France

<sup>2</sup>University of Arizona, 933 N. Cherry Ave, Tucson, AZ 85721

27 February 2012

## ABSTRACT

We examine the cosmic growth of the red sequence in a cosmological hydrodynamic simulation that includes a heuristic prescription for quenching star formation that yields a realistic passive galaxy population today. In this prescription, halos dominated by hot gas are continually heated to prevent their coronae from fueling new star formation. Hot coronae primarily form in halos above  $\sim 10^{12} M_{\odot}$ , so that galaxies with stellar masses  $\sim 10^{10.5} M_{\odot}$  are the first to be quenched and move onto the red sequence at  $z > 2$ . The red sequence is concurrently populated at low masses by satellite galaxies in large halos that are starved of new fuel, resulting in a dip in passive galaxy number densities around  $\sim 10^{10} M_{\odot}$  that agrees qualitatively with observations. Stellar mass growth continues for galaxies even after joining the red sequence, primarily through minor mergers with a typical mass ratio  $\sim 20\%$ . For the most massive systems, the size growth implied by the distribution of merger mass ratios is typically  $\sim 2\times$  the corresponding mass growth, consistent with observations. This model reproduces mass-density and colour-density trends in the local universe, with essentially no evolution to  $z = 1$ , with the hint that such relations may be washed out by  $z \sim 2$ . Our simulation produces a high red galaxy fraction at both high galaxy overdensity, independent of stellar mass, and high mass, independent of overdensity, suggesting quenching mechanisms associated with both environment and mass; in our model, both are connected to the presence of surrounding hot gas.

**Key words:** galaxies:evolution – galaxies:formation

## 1 INTRODUCTION

A substantial fraction of galaxies today inhabit a tight locus in colour-magnitude space known as the red sequence. Such galaxies typically have elliptical morphologies, have little or no star formation, little cold gas, and live in dense environments. They host the majority of stellar mass in the local universe (Hogg et al. 2002), and therefore are a critical population for understanding the global evolution of galaxies across cosmic time.

Despite a growing wealth of data, the origin of red sequence galaxies is still not fully understood. In the currently-favored cold dark matter (CDM) paradigm, massive galaxies should be surrounded by halos of hot gas that can potentially cool and fuel new star formation (White & Frenk 1991). Indeed many red sequence galaxies are seen to have measurable X-ray emission, directly indicating hot, cooling gas. Yet these galaxies show little cold gas or ongoing star

formation. Debate continues as to what physical mechanisms can halt star-formation and keep it halted for much of cosmic time with recent work favoring feedback from active galactic nuclei (AGN) as the primary energy source (e.g. Croton et al. 2006; Hopkins et al. 2008). But detailed observations have revealed more subtle complications – for instance, a significant fraction of red-sequence galaxies have a “frosting” of current star formation, though it contributes little to overall mass growth (Trager et al. 1998; Bower et al. 1998; Trager et al. 2008). Furthermore, while most massive red sequence galaxies are ellipticals, passive disks make up a large fraction at the low-mass end (Bundy et al. 2010; van der Wel et al. 2010). Assembling all these observations into a coherent framework for passive galaxy evolution has proved challenging.

More insight about the evolution of passive galaxies may be obtained by directly examining their history over cosmic timescales. This is now possible thanks to deep surveys that have placed constraints on the bright passive galaxy populations out to  $z \sim 1$  and even  $z >$

\* Email: jgabor@as.arizona.edu

2 (e.g. Bell et al. 2004; Faber et al. 2007; Brown et al. 2007; Cool et al. 2008; Kriek et al. 2008; Stutz et al. 2008; Taylor et al. 2009; Brammer et al. 2009; Marchesini et al. 2010; Whitaker et al. 2010). Ongoing surveys are expected to probe passive galaxies with stellar masses down to  $\sim 10^9 M_\odot$  (e.g. CANDELS; Grogin et al. 2011; Koekemoer et al. 2011). Current data indicates the bright end of the passive galaxy luminosity function has changed little (after correction for passive evolution) since  $z \sim 1$ , suggesting these galaxies were “in place” 7+ Gyrs ago. Furthermore, high-resolution imaging has revealed that passive galaxies are typically much smaller at  $z > 1$ , by factors  $\sim 5$  compared to their present-day descendants (Daddi et al. 2005; van Dokkum et al. 2008, 2010). These data likely provide strong constraints on passive galaxy formation models, but such constraints have yet to be fully explored in the context of hierarchical models.

Numerous physical processes are thought to contribute to the formation and evolution of passive galaxies, and many potential effects have proven difficult to rule out. Gas-rich galaxy mergers that induce a starburst and rapid black hole growth may drive the initial quenching of massive red galaxies (Springel et al. 2005; Hopkins et al. 2006, 2008). Alternatively, hot gaseous coronae that form in halos above  $\sim 10^{12} M_\odot$ , supplemented by additional heating from an active galactic nucleus (AGN) or another energy source, may starve galaxies of fuel for star-formation (Birnbom & Dekel 2003; Kereš et al. 2005; Dekel & Birnbom 2006; Croton et al. 2006; Cattaneo et al. 2006). Among satellite galaxies additional possibilities may drive quenching: starvation and/or ram-pressure stripping by hot intra-group or intra-cluster medium (ICM) may play a role, along with glancing interactions with other galaxies (Gunn & Gott 1972; Abadi et al. 1999; Quilis et al. 2000; Larson et al. 1980; Bekki et al. 2002; Richstone 1976; Moore et al. 1998). All these processes may act in combination to form passive galaxies as observed.

Once “red and dead,” the evolution of these galaxies may be deceptively complex. Although there is likely little or no new star formation, over its lifetime the stellar population sheds a significant fraction ( $\sim 1/2$ ) of its mass via stellar evolution (Jungwiert et al. 2001; Bruzual & Charlot 2003), providing an additional local source of gas. Furthermore, passive galaxies are subject to mergers and accretion of small satellite galaxies, which alter their stellar populations and add mass. Mergers can also alter galaxy structure (e.g. from disk ordered rotation to spheroidal random orbits) (Barnes 1990), change the characteristic size of the galaxy (Cox et al. 2006), strip stars into the ICM (Gallagher & Ostriker 1972; Murante et al. 2004), and possibly add cold gas. Such processes may all contribute to the observed evolution of the red sequence, and hypotheses addressing the observed *lack* of evolution must explain why these processes did not act or conspired to yield little evolution.

From a theoretical point of view, the challenge of galaxy formation is to assemble a collection of physical processes within a hierarchical structure formation scenario that yields the observed properties of both star-forming and passive galaxies at all redshifts. Recent work on star-forming galaxies suggests that their growth can be well-described as being fed by cold, filamentary accretion and regulated by strong galactic outflows (e.g. Davé et al. 2011b,a). Such processes are either observed and/or physically well-motivated. The

physics of the transition to red and dead galaxies is less well constrained, and it is unclear which of the many physical processes are driving this evolution. Cosmological hydrodynamic simulations that dynamically track these complex physical interactions offer a maturing framework for elucidating the key physical drivers, and simulations have now begun to explore the evolution of the passive galaxy population, particularly in connection with black hole growth (Di Matteo et al. 2005; Hopkins et al. 2006; Sijacki et al. 2007).

In this work, we study passive galaxy growth from high redshift until today using cosmological hydrodynamic simulations. These simulations incorporate physically-motivated but heuristic quenching mechanisms (described in Gabor et al. 2011) that yield a  $z = 0$  population of passive galaxies whose colour and luminosity distributions match observations. In particular, we include a prescription where we ensure that halos dominated by hot gas are continuously heated to keep circum-galactic gas hot. This simple and extreme prescription, approximating the effects of a heat source such as an AGN radio jet, successfully cuts off the fuel supply for star formation in massive halos which eventually yields passive galaxies. In contrast, we found in Gabor et al. (2011) that a quenching prescription based on major mergers alone fails to produce the observed properties of passive galaxies. Although significant challenges remain for our favoured model, it provides a general qualitative guide for models where hot massive halos are the main drivers of passive galaxy formation. While Gabor et al. (2011) focused on the  $z = 0$  red galaxy population and compared various quenching mechanisms, here we focus on our most successful quenching mechanism and its implications for passive galaxy evolution from high redshift until today, including environmental factors. Our model should not be considered physically correct in detail, but rather as broadly illustrative of the impact of some (unspecified) quenching mechanism that keeps hot halo gas hot on passive galaxy evolution over the past 10 billion years.

We begin by presenting an overview of our simulations in §2. Then we present our results, beginning in §3 where we examine number density and colour evolution, §4 where we look at how passive galaxies grow in mass and size via mergers, and §5 where we study mass and colour evolution versus environment. Finally, we summarize and discuss our conclusions in §6.

## 2 SIMULATIONS

### 2.1 Simulation methodology

We analyze the same cosmological hydrodynamic simulations described in Gabor et al. (2011). For completeness, we summarise the simulations here. They were run with an extended version of the N-body + smoothed particle hydrodynamics code GADGET-2 (Springel 2005). In addition to the basic N-body and hydrodynamics calculations, our version of the code includes sub-resolution modelling of gas cooling, star-formation, a model for chemical enrichment via AGB stars and both Type Ia and core-collapse supernovae, galactic winds associated with star-formation, and simple prescriptions for quenching star-formation.

We include both primordial and metal-line cooling assuming collisional ionisation equilibrium (Sutherland & Dopita 1993), with the metallicities self-consistently tracked within simulations; see Oppenheimer & Davé (2006, 2008) for details. We include heating from a metagalactic photo-ionising background (Haardt & Madau 2001), assuming all particles are optically thin. We truncate the cooling curve at  $10^4$  K because our simulations lack the resolution to properly model the interstellar medium; below this temperature, particles can only be heated or cooled via adiabatic expansion.

For star formation, we employ the two-phase model of Springel & Hernquist (2003) based on the analytic description of McKee & Ostriker (1977). Gas particles above a density threshold of  $0.13 \text{ cm}^{-3}$  are treated as cold, star-forming clouds embedded within a hot diffuse medium. The masses in the cold and hot phases are determined by the balance between evaporation by core-collapse supernovae and condensation. The star formation rate is then determined by the timescale over which cold clouds collapse into stars, and the model parameters are set so that the resulting star formation rates are consistent with the observed relation to surface gas density (Kennicutt 1998). Star-forming gas particles are converted into collisionless star particles stochastically, with a probability derived from the star formation rate. Gas particles may spawn up to two such star particles, conserving total mass.

As a gas particle is undergoing star formation, it self-enriches with metals from core-collapse supernovae. Furthermore, star particles share energy, mass, and metals with neighboring gas particles as a result of stellar mass loss from AGB stars and Type Ia supernovae. Stellar mass loss is calculated by assuming a Chabrier (2003) initial mass function, applying the stellar population models of Bruzual & Charlot (2003, , BC03), which account the mass lost by a stellar population at discrete times after the initial star-formation event. We use Type Ia supernova rates from Scannapieco et al. (2006), and each such supernova results in the production of metals (mainly iron) that are shared with neighboring gas particles. We note that in similar simulations, the predicted metallicities in hot gas around massive galaxies are in good agreement with observed values (Davé et al. 2008).

Our code further includes feedback in the form of galactic winds driven by star-formation (Oppenheimer & Davé 2006, 2008). Just as a star-forming gas particle has some probability of being converted into a star particle, it has a probability of being kicked in a wind, which is given by  $\eta$  (the mass loading factor) times the star formation probability. A wind particle is expelled from its host galaxy at a velocity  $v_w$  typically a few hundred  $\text{km s}^{-1}$ , and it is briefly decoupled from normal hydrodynamic interactions to approximate chimneys of escaping gas (Springel & Hernquist 2003). The velocities are chosen to match observations of local galaxy winds (Martin 2005; Rupke et al. 2005) and also match those seen at higher redshifts (e.g. Steidel et al. 2010). The mass loading factors scales as the inverse of the galaxy circular velocity, which is calculated from an on-the-fly galaxy finder (Oppenheimer & Davé 2008), and follows scalings as predicted for momentum-driven winds (Murray et al. 2005). With this prescription, our simulations match a broad array of observational constraints on star-forming galax-

ies and the intergalactic medium (Oppenheimer & Davé 2006, 2008; Oppenheimer et al. 2010; Davé et al. 2006, 2007; Finlator et al. 2007; Finlator & Davé 2008).

Despite their broad success, winds driven by star-formation generally do not result in the formation of red and dead galaxies. We incorporate an additional heuristic quenching model specifically to solve this problem (Gabor et al. 2011). For this model, we run a spherical overdensity algorithm on-the-fly to identify galaxy halos and separate gas above and below 250,000 Kelvin in each galaxy's halo. In halos with  $> 60\%$  of all gas above this temperature cutoff, we apply constant heating (at every time-step) to all circum-galactic halo gas to force it to remain at the halo virial temperature. Such heating could plausibly result from an AGN radio jet, but our model in fact uses more energy than thought to be available from observed AGN sources (Gabor et al. 2011). We exclude star-forming gas particles from this heating since a radio jet is unlikely to disrupt dense star-forming clouds on galactic scales. The heating we apply to circum-galactic gas is sufficient to prevent it from condensing onto the galaxy, thus starving the galaxy of new fuel for star-formation. This model results in a bimodal colour distribution of galaxies, and red galaxy luminosity functions that match observations of the local universe. Although the model has some difficulties (like the required energy mentioned above), it should be a good representation of models where galaxies are quenched due to starvation enabled by their surrounding hot coronae.

## 2.2 Runs and galaxy identification

For this paper, we employ a simulation of a  $48h^{-1}$  comoving Mpc random cosmological cube with  $256^3$  dark and  $256^3$  gas particles that incorporates all the above physics. We use a *Wilkinson Microwave Anisotropy Probe* concordance cosmology (Komatsu et al. 2009) with  $H_0 \equiv 100h = 70 \text{ km s}^{-1} \text{ Mpc}^{-1}$ , matter density  $\Omega_m = 0.28$ , baryon density  $\Omega_b = 0.046$ , a cosmological constant with  $\Omega_\Lambda = 0.72$ , root mean square mass fluctuation at separations of 8 Mpc  $\sigma_8 = 0.82$ , and a spectral index of  $n = 0.96$ . Our simulation uses a gravitational softening length of  $3.75h^{-1} \text{ kpc}$ . The initial gas particle mass is  $1.2 \times 10^8 M_\odot$ , the typical star particle mass is half that, and our simulation results in  $\sim 3000$  resolved galaxies at  $z = 0$ .

We save snapshots of the simulation at 108 redshifts, starting at  $z = 30$  and ending at  $z = 0$ . The time between snapshots ranges from a few tens of Myrs at high redshift to  $\sim 300$  Myr at low redshift. The snapshots contain information for simulation particles, such as position, velocity, mass, metallicity, gas density, gas temperature, and star-formation rate. From these particle data, we determine galaxy properties to compare with observables.

We use `Skid`<sup>1</sup> to identify galaxies (cf. Gelb & Bertschinger 1994; Kereš et al. 2005). `Skid` provides a list of member particles (star and star-forming gas) for each simulated galaxy. The sum of member star particle masses is then the galaxy stellar mass, and the instantaneous star formation rates of the gas particles are summed to give the star formation rate of the galaxy.

<sup>1</sup> <http://www-hpcc.astro.washington.edu/tools/skid.html>

We then calculate galaxy spectra using the models of Bruzual & Charlot (2003), as in Finlator et al. (2006). We treat each star particle as a single stellar population with an age and metallicity determined directly in the simulation. By adding up the spectra of all star particles within a galaxy, we obtain the spectrum of that galaxy, from which we measure galaxy colours and magnitudes in various bands. Though we focus on the passive galaxy population that is thought to be mostly dust-free, when considering star-forming galaxies we sometimes include a prescription for dust obscuration following Finlator et al. (2006).

### 2.3 Building merger trees

Beyond knowing galaxy properties at a given redshift, we wish to study the histories of individual galaxies as they evolve. For this we must connect each galaxy at  $z = 0$  to its progenitor galaxies at earlier redshifts: i.e., build a merger tree. We do so by determining, for every star particle in a given galaxy, which galaxy from an earlier snapshot that star particle lived in. If the star formed recently it wouldn't have lived in any previous galaxy. By tracing star particles in this way, we determine the immediately preceding progenitors of each galaxy. Galaxies with multiple progenitors must have undergone a merger (or at least some galaxy interaction, such as stellar stripping).

Creation of a merger tree from a cosmological simulation involves handling a number of pathological circumstances owing to the stochastic nature of the gas and star particles. A common annoyance is that if two galaxies fly by each other in a close encounter, *Skid* (and most other galaxy finders) will often identify them as a single galaxy during one or a few timesteps, but then again as separate galaxies at later times. More rarely, a group of stars that make up a galaxy at one timestep may be assigned to no galaxy at all in a subsequent timestep (i.e. they are part of the intracluster light), giving the appearance that a galaxy disappeared. This can happen with quite large galaxies ( $> 1000$  particles). While these issues do not affect the majority of galaxies and hence do not strongly impact the overall results, they must nevertheless be handled in an appropriate manner.

To surmount these difficulties, we follow strategies described in Maller et al. (2006), who dealt with the same issues. We distinguish *Skid* groups from galaxies, the latter being defined in terms of our merger trees. For each star particle in a *Skid* group at  $z = 0$ , we trace the history of its host *Skid* groups over all timesteps. If the star particle does not appear in any *Skid* group during some timestep, then we assign it to a virtual group where it is the only member. We then assign each group (real and virtual) to a galaxy. At the highest-redshift timestep of interest, each *Skid* group is defined as a separate galaxy. In the subsequent timesteps, each group is assigned to the same galaxy as its most massive progenitor from the immediately preceding timestep. Thus if two separate *Skid* groups share the same progenitor, then they are both assigned to the same galaxy, even though *Skid* would identify them as separate. This helps handle the case where two merging galaxies undergo a close passage, then separate before the final merger. Note that the precise timing of final coalescence may be incorrect by up to  $\sim 1$  Gyr, but our results do not rely on this timing aspect. Likewise, virtual groups that were not part of any *Skid* groups are as-

signed to galaxies that they once inhabited. Once all groups are assigned to galaxies, their constituent particles can also be assigned to those galaxies.

The above prescription assumes that once galaxies are joined by *Skid*, they will eventually merge. But some fly-by interactions will not lead to mergers. To account for this, we identify galaxies at  $z = 0$  that are composed of multiple *Skid* groups and separate those groups into distinct galaxies. We find the earliest timestep when both groups' stars are assigned to the same galaxy, and from then on assign a new galaxy ID to those stars in the smaller of the two groups. With every star particle assigned to a galaxy at every timestep, we then identify all progenitor galaxies to each galaxy.

### 2.4 Environment measures

In order to study *where* red galaxies emerge in our simulation, we measure the local galaxy density around *Skid* galaxies. We use two density measures. An intuitive and simple approach is to count the number of simulated galaxies within  $1h^{-1}$  Mpc of the galaxy of interest (Blanton 2006). For some purposes this measure too noisy, as it places galaxies into discrete bins of density, and some galaxies have few neighbors within  $1h^{-1}$  Mpc. Thus, as an alternative we use *Smooth*<sup>2</sup>, which calculates the mean density at each galaxy's location after smoothing over the nearest 16 galaxies with a spline kernel (similar to an SPH density calculation). This allows us to quantify low densities less stochastically than by simply counting galaxies within some fixed distance. In some cases we use a galaxy's local overdensity to compare with observations: the overdensity is measured relative to the mean resolved galaxy density in our simulation volume.

## 3 EVOLUTION IN COLOUR AND NUMBER DENSITY

### 3.1 Color-mass diagrams and stellar mass functions

Recent observations enable two simple but powerful constraints on the emergence and evolution of passive galaxies: their colours and number densities. In this section we examine how colours and number densities (parameterized via the galaxy stellar mass function) evolve with redshift in our simulations. We note that our simulations do not perfectly match present-day observations of passive galaxies, as detailed in Gabor et al. (2011); for instance, the colors are slightly too blue and the red sequence does not have the correct slope (likely a metallicity effect). Nonetheless, our simulations clearly identify two general trends in passive galaxy evolution: (1) the first passive galaxies emerging at  $z > 2$  are at the massive end of the galaxy stellar mass function, followed shortly by small satellites, then finally the middle region of  $10^{10} M_{\odot}$  galaxies. (2) The most massive red galaxies in our model grow substantially at late times.

Figure 1 shows colour-mass diagrams and galaxy stellar mass functions for simulated galaxies at redshifts 0, 0.3, 1, and 2. The  $g-r$  colours are rest-frame SDSS filter bands, and

<sup>2</sup> <http://www-hpcc.astro.washington.edu/tools/smooth.html>

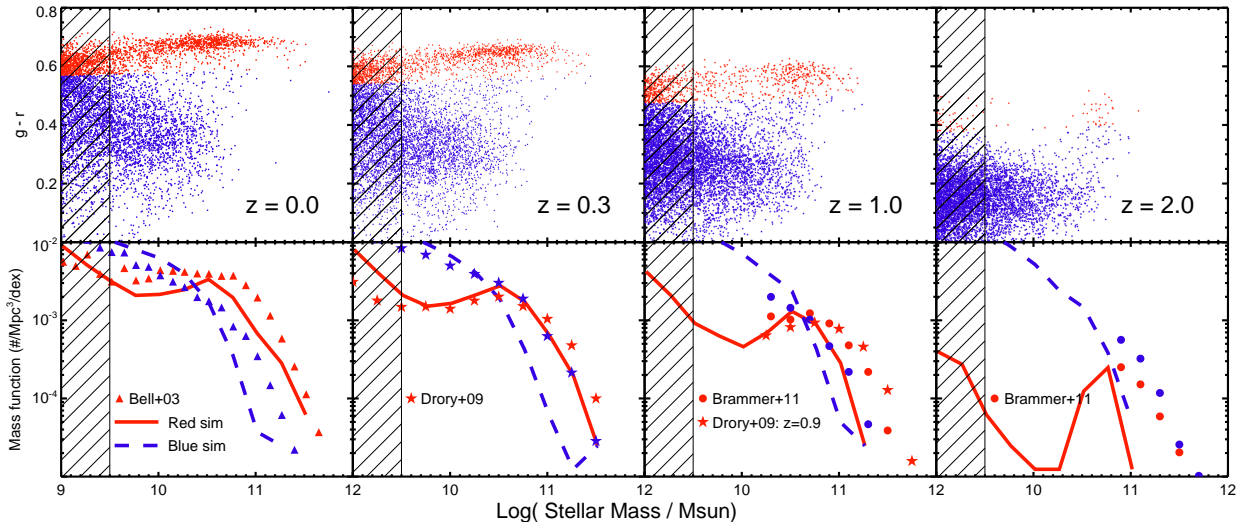


**Figure 1.** Redshift evolution of colour-mass diagrams (top row) and galaxy stellar mass functions (bottom row). Redshift increases from left to right, as labeled. Red and blue galaxies are separated using a redshift-dependent cut, as illustrated by the red and blue colour-coding in the CMD. In the mass function panels, solid lines denote the simulated red sequence, dashed lines the simulated blue cloud, and observed data points are taken from the literature. The hatched region indicates poorly resolved galaxies. Massive red galaxies are present at  $z = 2$ , but not in sufficient numbers compared to observations. There is a dearth of intermediate mass galaxies ( $\sim 10^{10} M_{\odot}$ ) that is more pronounced at higher redshifts.

do not include any correction for obscuration due to dust – these are intrinsic colours. We divide the galaxy population into blue and red using a straight line in  $g-r$  colour versus  $r$  magnitude space in the same way as in Gabor et al. (2011). This translates to a similar separation in colour-mass space, as indicated by the sharp demarcation between blue and red points in the top left panel. We evolve the normalization (but not the slope) of our colour separation in a simple linear way that approximately accounts for passive evolution:  $y_{\text{sep}}(z) = y_{\text{sep}, z=0} - 0.1 * z$ . Here  $y_{\text{sep}}$  is the y-intercept (i.e. colour) of the line of separation, and  $z$  is the redshift. The resulting separation indicated by the colour-coding of blue and red galaxies in the top panels of Figure 1 suggests this is a reasonable choice. The hatched region on the left of the figure denotes the mass range of galaxies that may be inadequately resolved.

The colour evolution of the galaxy population is clear from the figure. The main feature is the strong growth in the passive galaxy population from  $z = 2 \rightarrow 0$ . The blue galaxy population also becomes redder with time, at roughly the same rate as the red sequence. This indicates that even galaxies in the blue cloud have their colour evolution driven by passive stellar aging. Recall that we do not include extinction here, but particularly at high redshifts, many of the blue galaxies may lie in the red region had we included dust; this complicates comparisons with observations, which typically have difficulty separating these populations (passive vs. dusty star-forming) at higher redshifts.

The lower set of panels of Figure 1 shows galaxy stellar mass functions separated into blue (dashed line) and red (solid line) populations. We plot mass function observations taken from Bell et al. (2003), Drory et al. (2009), and Brammer et al. (2011), who likewise split galaxies into star-forming and quiescent populations (red vs. blue points), though with slightly different criteria. We note that our sim-

ulated mass function has too few massive galaxies, but approximately the correct shape at  $z = 0$  (increasing all stellar masses by  $\sim 50\%$  provides a good match). Although this model provides a good match to the luminosity function of red galaxies at  $z = 0$  (Gabor et al. 2011), the corresponding masses of these galaxies are too small, indicating a problem with their mass-to-light ratios. Increasing the hot gas fraction above which we apply quenching from the value of 60% used here can effectively shift the mass function to higher masses (Gabor et al. 2010) and may provide better agreement with this data, though likely at the expense of the luminosity function agreement. These small differences notwithstanding, we are mostly interested in the evolution of the red sequence, and hence we focus on qualitative aspects of this model rather than tuning to match observables.

From the figure we see that the simulated blue galaxy stellar mass function evolves only weakly with redshift, but the red galaxy mass function obviously undergoes drastic growth from  $z > 2$  to 0. The rapid buildup of passive galaxies reflects the quenching of star-forming galaxies due to starvation in our model (see Gabor et al. (2011)). The red sequence grows from mostly non-existent at  $z \sim 3$  to dominating the galaxy population at  $z \sim 0$ . The mass functions clearly show that the most massive galaxies are the first to become red, followed by low-mass galaxies that turn out to be satellites to the massive ones. This directly results from the fact that the most massive galaxies in our simulations are the first to form a corona of hot gas. Massive galaxies tend to live in massive dark matter halos, and massive dark matter halos have low enough densities that virial shock heating outpaces radiative cooling, allowing a hot gaseous halo to develop (Birnboim & Dekel 2003). We note that our simulation volume is limited, so that we are likely underestimating the prevalence of the most massive systems that

would be the very first ones to become passive at the highest redshifts.

### 3.2 A dearth of passive galaxies at $M_* \sim 10^{10} M_\odot$

Examining the red sequence growth in more detail, we find that the first passive galaxies form at the massive end by  $z \approx 3$ , which is likely a lower limit since our limited simulation volume does not capture the most massive structures in the Universe. Soon thereafter, small satellites of the first quenched galaxies become red as well, owing to starvation of gas in growing hot halos (Simha et al. 2009). Intermediate-mass galaxies with  $M_{\text{stellar}} \approx 10^{10} M_\odot$  are the last to quench, filling in the gap between the centrals and satellites such that by  $z \sim 0$  this bimodality within the red sequence is not so evident. Therefore, a strong prediction of this quenching mechanism is that there is a distinct gap between the massive and low-mass ends of the red sequence that becomes more pronounced with redshift.

Galaxies around  $10^{10} M_\odot$  at  $z \gtrsim 1$  are typically neither massive enough to support their own hot coronae, nor close enough to larger galaxies to live in the hot gas environment of a (proto-)group or cluster. By redshift zero, however, many galaxies within this mass range live in halos dominated by hot gas due to the presence of very massive neighbors. As we will discuss further in § 5, at times they may not even occupy the same virialised halo, but rather live in a nascent super-structure with pervasive hot gas that triggers quenching.

The increasingly prominent dip in the red galaxy mass function at  $M_* \sim 10^{10} M_\odot$  to higher redshifts is consistent with existing observational constraints. Stutz et al. (2008) found six massive ( $> 10^{10.4} M_\odot$ ) but zero low-mass galaxies with old stellar populations at  $z \sim 3$  in the Hubble Ultra-Deep Field (HUDF; Beckwith et al. 2006), despite being sensitive to stellar masses below  $10^{10} M_\odot$  (see also Toft et al. 2005). Rudnick et al. (2009) noted that in clusters, the low mass end of the mass function must build up more rapidly than the massive end from  $z \sim 0.8$  to  $z = 0$  in order to “catch up” in number density. In the field, Drory et al. (2009) traced the evolution of the red galaxy stellar mass function for  $z < 1$ , finding a dip at medium masses that is more prominent at higher redshift; some of these data are plotted in Figure 1. Similar trends have been noted at low redshift (e.g. Baldry et al. 2008). Our simple model, where hot gas dictates the formation of the red sequence, provides a compelling physical picture behind this trend, which we describe next.

### 3.3 Central and satellite evolution along the red sequence

The separation in mass range between central and satellite galaxies along the red sequence is more pronounced at earlier epochs, leading to a sort of bimodality along the red sequence itself. This is naturally understood within a hierarchical structure formation model, as we outline here.

In our model, the initial emergence of the massive red sequence is directly tied to the requirement that a galaxy’s halo be dominated by hot gas for quenching to begin. Early spherically-symmetric analytic models of

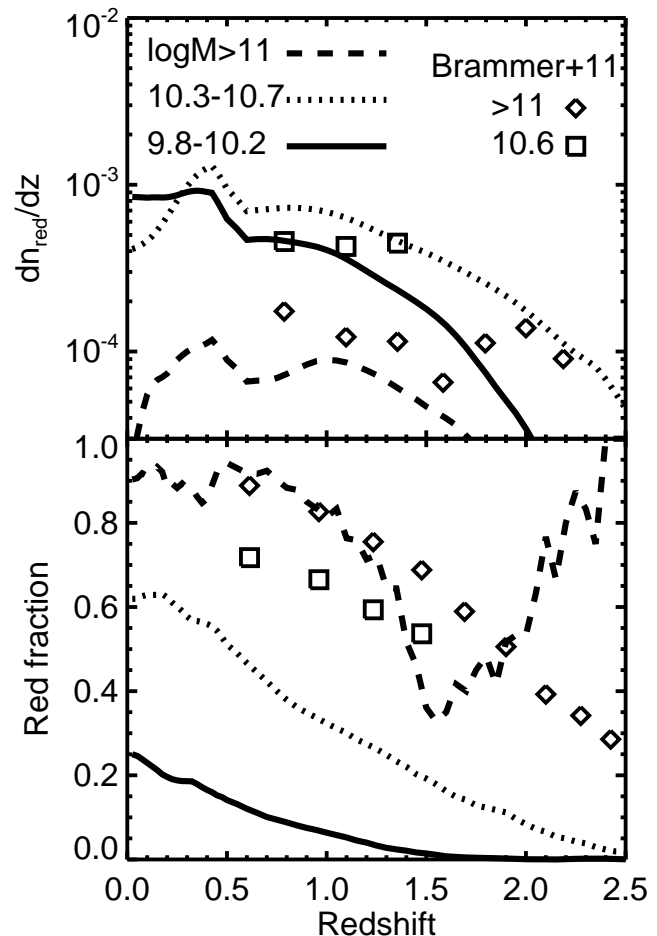


**Figure 2.** **Top:** Rate of change of red galaxy number density with respect to redshift, for three stellar mass bins (solid, dotted, and dashed lines). We compare to smoothed derivatives based on data from Brammer et al. (2011), squares and diamonds for two mass bins. At  $z < 0.5$  in our model, the number of low-mass galaxies starts to catch up to the number of more massive (middle bin) galaxies, as the derivative there is higher for low-mass galaxies. **Bottom:** Red galaxy fraction as a function of  $z$  for the same three bins in stellar mass, again with data from Brammer et al. (2011). Our model under-predicts the observed red galaxy fraction at  $M < 10^{10.7}$ .

galaxy evolution assumed that gas in the halo of a forming galaxy should be virialised (Rees & Ostriker 1977; Silk 1977; White & Rees 1978). It was realised, however, that gas in low-mass halos will have short cooling times, so that it never reaches the virial temperature of the halo (Binney 1977; White & Frenk 1991; Binboim & Dekel 2003). Several recent hydrodynamic studies have shown that a hot circumgalactic corona only forms, via the virial shock, in halos above a few  $\times 10^{11} M_\odot$  (Kereš et al. 2005; Binboim & Dekel 2003). These analyses neglected metal-line cooling, which is particularly important in massive hot halos that are heavily enriched (Davé et al. 2008). Our simulations including metal-line cooling indicate a higher mass threshold of  $\sim 10^{12} M_\odot$  for a hot corona to form (Gabor et al. 2010). In accord with previous analyses, we find that this threshold does not evolve significantly with redshift.

The key assumption in our model is that in such hot-gas dominated halos, gas is very inefficiently deposited onto the galaxy, likely owing to the contribution of some preventive feedback process(es) like AGN heating (e.g. Dekel & Birnboim 2006; Croton et al. 2006; Cattaneo et al. 2006; Bower et al. 2006; Birnboim et al. 2007). Since galaxy stellar masses are well-correlated with halo masses below the cutoff for quenching, only central galaxies with the highest stellar masses will live in hot halos at early times.

As the universe evolves, more galaxy halos become large enough to support hot coronae. Massive central galaxies thus continue to move onto the red sequence. Our hot gas fraction cutoff of 60% roughly corresponds to a stellar mass of about  $10^{10.5} M_\odot$ , though there is significant scatter. Once galaxies exceed this stellar mass, they will tend to migrate toward the red sequence over the span of 1 – 2 Gyr. We note that this mass cutoff is unlikely to be correct at  $z \gtrsim 2$ , since there are seen to be a number of star-forming galaxies seen with stellar masses approaching and even exceeding  $10^{11} M_\odot$  (e.g. Daddi et al. 2007). Simulations by Dekel et al. (2009) suggest that at these redshifts, dense cold inflow can penetrate hot halos and therefore fuel star formation even in the presence of a hot corona. At lower redshifts, this phenomenon is expected to weaken considerably (Kereš et al. 2009), and thus our quenching model may be more appropriate for  $z \lesssim 2$  or perhaps  $z \lesssim 1.5$  passive galaxies.

What happens with satellite galaxies? The halo occupancy of small halos is typically unity (e.g. Berlind et al. 2003), that is, small halos tend to be dominated by a single central galaxy with only very small satellites present. This is because the cold accretion that feeds galaxy growth tends to bypass satellites, thereby disproportionately growing the central object. When such a central galaxy becomes quenched, it satellites also undergo quenching by starvation owing to the growth of the same hot halo that triggers our quenching mechanism. But these satellites are quite small, and therefore initially populate the very low-mass end of the red sequence, leaving a strongly bimodal mass distribution of passive galaxies.

These quenched halos then merge with nearby halos owing to hierarchical growth. As the smaller halo falls in, its central galaxy becomes a satellite and is quenched by the hot ICM on a 1 – 2 Gyr timescale (Simha et al. 2009). These infalling (former) central galaxies are typically larger than the original satellites within the quenched halo, and hence begin to populate the intermediate-mass portion of the red sequence. They of course also bring in additional low-mass satellites. Therefore as time progresses, hierarchical growth combined with starvation by the hot corona results in a gradual “filling in” of the intermediate-mass red sequence. These trends will be explored in more detail, particularly in relation to environment, in §5.

Recent semi-analytic models by De Lucia et al. (2011) analogously found a bimodality in elliptical galaxy masses with a minimum at  $M_{\text{stellar}} \sim 10^{10} M_\odot$ . They argue that this arises in their model owing to mergers probabilities increasing with mass and disk instabilities contributing to bulge growth. Our simulations yield qualitatively similar results, but in our case passive galaxy formation is not driven by mergers or instabilities, but rather by starvation by a hot halo. It is worth noting that their model is geared towards producing elliptical morphologies, while ours is focused on

producing passive systems, which are highly overlapping population in the real Universe but may arise from different physical mechanisms (and not exactly coevally; Bundy et al. 2010). It would be interesting to compare and develop discriminating predictions for these scenarios; we leave this for future work.

### 3.4 Red galaxies undergo strong evolution

Figure 2 illustrates the evolutionary trends in passive galaxy number density more explicitly. We consider three bins in stellar mass, and show how the number density of passive galaxies in each bin changes with redshift via the derivative  $dn_{\text{red}}/dz$ . Passive galaxies with masses between  $10^{10.3}$  and  $10^{10.7} M_\odot$  are the most numerous at all epochs, and experience the highest growth rate over most of the history of the universe. Less massive galaxies with  $M_{\text{stellar}} \sim 10^{10} M_\odot$ , i.e. within the “gap” in the mass function, emerge later but their growth rate accelerates to later epochs, being higher than more massive galaxies at  $z < 0.5$ . This illustrates the catch-up growth in the numbers of middle mass galaxies. Finally, red sequence galaxies more massive than  $10^{11} M_\odot$  are formed owing to migration from the lower-mass bins as they acquire mass through mergers, which is a relatively slow process, and hence their growth rate is the slowest.

Comparison between simulated and observed red galaxy mass functions (Bell et al. 2003; Drory et al. 2009; Brammer et al. 2011) in Figure 1 shows that our model under-predicts the numbers of massive ( $> 10^{11} M_\odot$ ) red galaxies, increasingly so at higher redshifts. In the real Universe, significant populations of massive red galaxies exist at  $z \gtrsim 2$ , and they grow appreciably in number since that epoch (but growth is modest from  $z \sim 1$  to  $\sim 0.3$  Brown et al. 2007; Cool et al. 2008; Taylor et al. 2009; Brammer et al. 2011). To quantify the discrepancy between observations and our simulation in Figure 2, we also show smoothed observational number density growth rates for two mass bins derived from the absolute number density measurements of Brammer et al. (2011, squares and diamonds). This confirms that the growth rate of the largest passive galaxies is somewhat too low in our simulations.

The bottom panel of Figure 2 shows the fraction of galaxies that are red in different mass bins as a function of redshift. Again we include data from Brammer et al. (2011). At  $z \lesssim 1.5$  our simulation matches the observations well for the most massive galaxies only. The simulation underpredicts the red fraction for galaxies less massive than  $10^{10.7} M_\odot$ , probably due to an excess of blue star-forming galaxies at these lower masses.

To summarise the last few sections, our model predicts that galaxies with  $M_{\text{stellar}} \sim 5 \times 10^{10} M_\odot$  are the first to become passive, but it underpredicts the numbers of galaxies with  $M_{\text{stellar}} > 10^{11} M_\odot$ . Galaxies in the “gap” at  $M_{\text{stellar}} \sim 10^{10} M_\odot$  catch up with time. The key feature driving these trends is that our quenching mechanism, tied to the hot gas coronae that form in halos  $\sim 10^{12} M_\odot$ , selects a characteristic mass for passive galaxies. That is, once a star-forming galaxy achieves a mass  $\gtrsim 10^{10.5} M_\odot$ , it will become quenched and move to the red sequence. Less massive galaxies are only quenched as satellites (or nearby halos) of more massive halos. More massive galaxies can only be obtained via merging. While quantitative details may vary



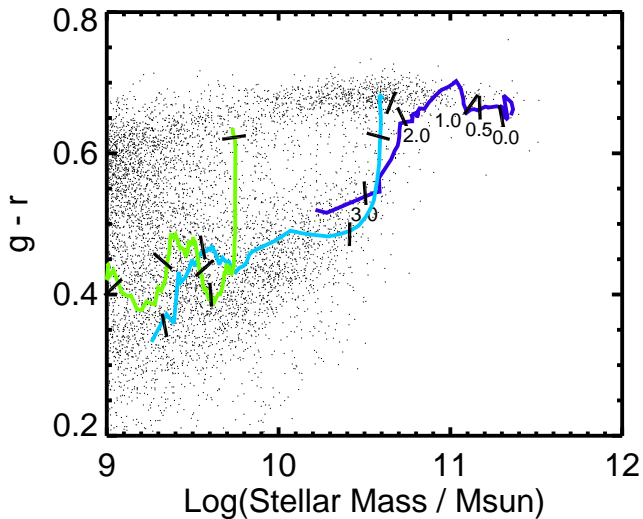


**Figure 3.** Example evolutionary paths in the colour-mass diagram. We show the paths of three galaxies (coloured lines) as they evolve through the colour-mass diagram, as represented by  $z = 0$  galaxies (small points) in the background. This is analogous to the schematic diagram of Faber et al. (2007). Both background galaxies and paths include a prescription for dust obscuration, and paths are corrected for passive colour evolution. Black lines indicate redshifts along the evolutionary paths, as labelled for the most massive galaxy. Galaxies grow in stellar mass along the blue sequence, then move vertically to the red after quenching. Once on the red sequence, galaxies grow only via mergers and accretion of satellites. Such growth can be substantial, as for the path of the most massive galaxy shown.

with parameter choices, these are generic outcomes for hierarchical quenching models keyed to a critical halo mass.

### 3.5 Paths to the red sequence

Here we focus on the path of individual galaxies in colour-mass space: Given a red galaxy at  $z \sim 0$ , what path did it take to get there? It turns out that massive galaxies in our models follow paths much like those in the schematic diagram of Faber et al. (2007): they move onto the red sequence at masses near the turnover in the mass function, then grow further through mergers and accretion of satellite galaxies.

In Figure 3 we show the paths of three typical galaxies (coloured lines) in the colour-mass diagram. We plot a background of simulated galaxies at  $z = 0$  (points), and we correct for passive evolution of colours for the galaxy paths in the same way that we evolved our line separating blue and red galaxies §3.1. Here we also include a simple prescription for dust that is tied to the star-formation rate of each galaxy (Somerville et al. 2001; Wang & Heckman 1996; Gabor et al. 2010).

All three of these galaxies build stellar mass via star-formation for several Gyrs before moving onto the red sequence. Once quenched, they stop building stellar mass and cross vertically and rapidly over the green valley to the red sequence in  $\lesssim 2$  Gyr (see the star-formation histories in

Gabor et al. 2011). The two less massive galaxies make this transition at late times ( $z < 0.5$ ), and do not change in mass or colour after reaching the red sequence because they do not have time to undergo mergers.

The most massive galaxy, in contrast, reaches the red sequence at  $z \sim 2$  when its mass is a few  $\times 10^{10} M_{\odot}$ , and then continues to grow in mass along the red sequence via mergers, eventually obtaining a mass of  $\sim 10^{11} M_{\odot}$ . The colour evolution along the red sequence is generally towards the blue (when corrected for stellar evolution), by virtue of accretion of smaller galaxies that are typically less red owing to lower metallicities. This is the basic reason why, as we showed in Gabor et al. (2011), the predicted red sequence slope is too shallow and does not match the observed red sequence slope, particularly at the massive end. Given that our star-forming galaxies lie on the mass-metallicity relation (Finlator & Davé 2008; Davé et al. 2011a), it is difficult to envision ways to avoid this natural consequence of merging. One possibility is that the amount of merging is overestimated in our models, perhaps because interactions in the real Universe result in satellites being stripped into the ICM rather than joining the central galaxy. If so, intracluster light is predicted to have significantly lower metallicities than the central galaxy; this is difficult to test observationally at present. Another possibility is that there are too many low-mass galaxies at early epochs in our models, as comparisons to high- $z$  mass functions preliminarily suggest (Davé et al. 2011b), which provides excess fodder for late-time merging. Clearly the detailed evolution of the most massive systems is not fully vetted in our current simulations.

More broadly, these paths are fairly representative for galaxies in their respective mass ranges. Low-mass galaxies tend to move onto the red sequence at late times, and grow little after doing so, while massive galaxies become passive at earlier epochs and grow in mass by merging with smaller galaxies.

### 3.6 Specific star formation rates

A key observational constraint on the transition of galaxies onto the red sequence is provided by the distribution of specific star formation rates (sSFR) versus stellar mass. This contains similar information to the colour-mass plots above, but here we additionally compare our current quenching simulations with previous similar runs without quenching from Davé et al. (2011b). We particularly examine the stellar mass range over which the transition to passive occurs, since the observed lack of a sharp delineation in stellar mass between passive and star-forming galaxies has been used as an argument against a quenching prescription based on halo mass (as ours is, approximately).

Figure 4 shows sSFR as a function of stellar mass for a simulation without any quenching (green points) and the halo quenching run presented in this paper (red). Blue lines show a running median for each. Galaxies with  $\text{sSFR} \leq 10^{-3} \text{ Gyr}^{-1}$  are shown along bottom of the plot. The no-quenching run employs the same cosmology, volume, input physics (besides quenching), and outflow model. But it has more particles ( $2 \times 384^3$ ), and consequently has somewhat better mass and spatial resolution, and hence its resolved galaxy population extends to slightly lower masses.



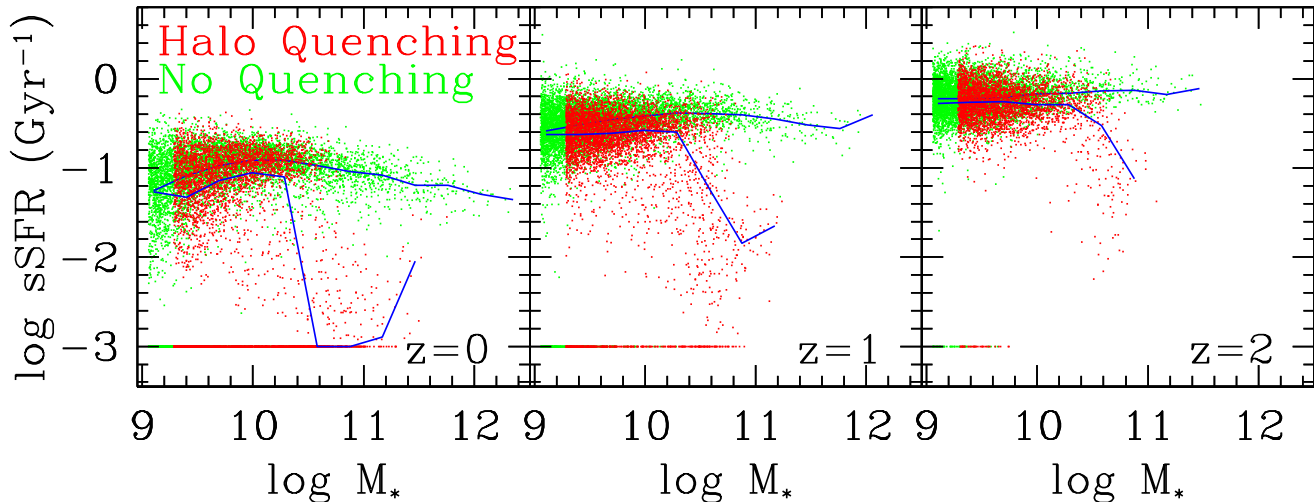


**Figure 4.** Specific star formation rate (sSFR) as a function of stellar mass at redshifts 0 (left), 1 (middle), and 2 (right). Red points correspond to our halo quenching model and green points to a simulation without quenching. Blue solid lines show the running median sSFR for both models. Many quenched galaxies have no star-formation, so we assign a minimum sSFR of  $10^{-3} \text{ Gyr}^{-1}$ . Quenching has little impact on the sSFR- $M_*$  relation below  $\sim 10^{10.5} M_\odot$ , but causes a drop in sSFR above this threshold at all redshifts. The transition quenching mass is blurred by satellite galaxies  $\sim 10^{10} M_\odot$  becoming quenched.

The form and evolution of the sSFR for the non-quenched case is discussed extensively in Davé et al. (2011b). Key points are that the relation is flat at high- $z$  moving towards a mildly negative slope by  $z \sim 0$ , sSFR increases with redshift at a given stellar mass steadily out to  $z = 2$ , and the scatter is typically  $\sim 0.2$  dex or less. The relation fundamentally arises from gravitationally-driven smooth cold accretion that dominates galaxy fueling, and diminishes with time as the Universe expands (e.g. Davé 2008).

The impact of halo quenching is clearly seen at masses  $\gtrsim 3 \times 10^{10} M_\odot$ . Below this transition mass, there is a minimal difference in the quenched and non-quenched relations, never exceeding a difference of more than 0.2 dex in the median: at these masses, star-forming galaxies still dominate the number densities of galaxies. Above this transition mass, the sSFR drops quickly towards small values, which is qualitatively similar to observations (e.g. Salim et al. 2007). The transition mass evolves very little with redshift, being only marginally higher at  $z \sim 2$ , which reflects the fairly constant relation between halo mass and stellar mass in these simulations. At all redshifts, the highest mass galaxies are still forming stars at a non-trivial rate, though much reduced relative to the no-quenching case. This partly reflects the infall of satellites that have not fully quenched onto the central (quenched) object. Tracking the evolution of these objects in detail is a difficult problem particularly for SPH (e.g. Agertz et al. 2007), and hence the upturn in sSFR at the highest masses should be taken with some caution. Nevertheless, it is clear that quenching as implemented in our simulations has a dramatic impact on the sSFR of galaxies above the transition mass of  $3 \times 10^{10} M_\odot$ , where many galaxy properties are observed to undergo a strong transition (Kauffmann et al. 2004). In our model there are very few galaxies above this mass on the main star-forming sequence, and SAMs with similar quenching

mechanisms suggest this behavior disagrees with observations (Somerville et al. 2008)

Particularly noteworthy are the intermediate-mass galaxies that we argued earlier are “filling in” the gap of the red sequence at stellar masses of  $\sim 10^{10} M_\odot$ . As we will argue in § 5, these galaxies are a combination of large satellites and centrals that are below the quenching threshold but have been quenched owing to living in a hot large-scale environment. As these galaxies become more numerous towards lower redshifts, the transition between quenched and unquenched is significantly blurred, such that many quenched galaxies are present at masses below the nominal transition mass. Hence the argument that the observed gradual transition from unquenched to quenched galaxies rules out a model based on halo mass quenching (which our model approximates) may not be justified. While our simulations qualitatively resemble observations, it is worth noting that such environmental quenching processes are not as robustly modeled as we would like in our simulations, and hence a more quantitative comparison will have to await improved modeling of the interactions of galaxies moving through hot halo gas.

## 4 GROWTH ALONG THE RED SEQUENCE

### 4.1 Mergers since quenching

We have seen that a galaxy does not stop growing and evolving once it reaches the red sequence (see Figure 3). Its existing stellar population ages, that population sheds mass via stellar winds, and it obtains new stars (and gas) via mergers. Here we show that the most massive galaxies, which are quenched at early times ( $z > 1$ ), often grow by factors of a few between quenching and the present day. In contrast, low-mass red galaxies (mostly satellites) tend to lose mass

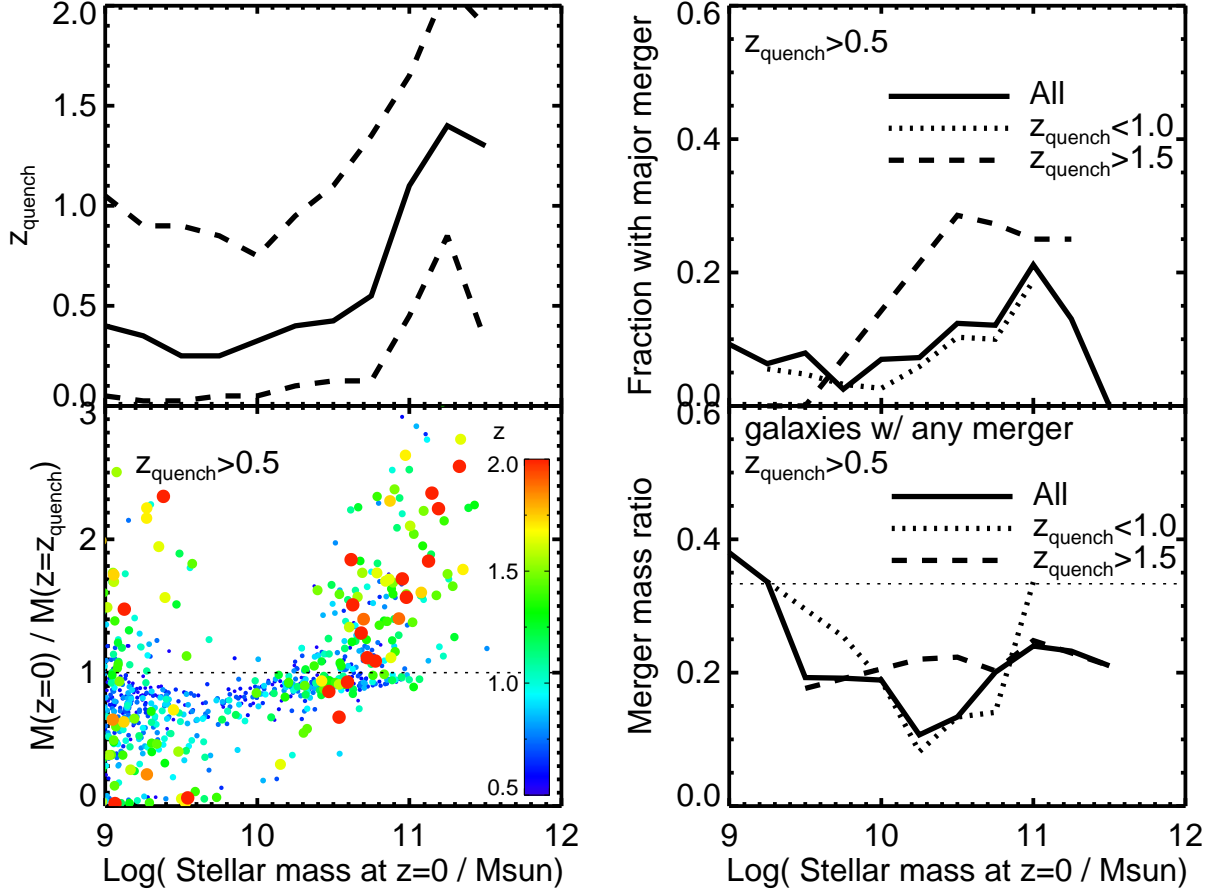


**Figure 5.** Growth of galaxies along the red sequence. In our model, the most massive galaxies typically grew by factors of a few since being quenched at  $z \sim 1$ , and that mass growth is dominated by minor mergers. **Top Left:** median (solid line), 10th and 90th percentiles (dashed) of the redshift at which red sequence galaxies were quenched ( $z_{\text{quench}}$ ) in different mass bins. **Bottom Left:** fractional mass growth of red sequence galaxies since  $z_{\text{quench}}$ , as a function of stellar mass at  $z = 0$ , among galaxies quenched before  $z = 0.5$ . Galaxy points are colour-coded by  $z_{\text{quench}}$ , and galaxies with higher  $z_{\text{quench}}$  have larger symbol sizes. **Top Right:** the fraction of galaxies per bin that have undergone at least one major merger since being quenched, among galaxies with  $z_{\text{quench}} > 0.5$ . The fraction for galaxies with  $0.5 < z_{\text{quench}} < 1.0$  (dotted) is typically lower than that for galaxies quenched earlier,  $z_{\text{quench}} > 1.5$  (dashed). **Bottom Right:** the mass-weighted average merger mass ratio, among galaxies with  $z_{\text{quench}} > 0.5$ . The mean merger is always a minor merger ( $< 1/3$ , thin dotted line). Galaxies quenched at high redshifts (dashed line) all have a merger mass ratio of  $\approx 0.2$ , while those quenched at somewhat lower redshifts (dotted) show stronger variation with mass.

through stellar evolution and stripping without undergoing significant mass growth via mergers.

The top left panel of Figure 5 shows the distribution of the redshift at which galaxies are quenched,  $z_{\text{quench}}$ , as a function of the final stellar mass at  $z = 0$ . We plot the 50th (solid), 10th, and 90th percentiles (dashed) of the distribution in each bin. The quenching redshift is defined as the redshift when a galaxy first appears red in the colour-magnitude diagram, with an evolving dividing line between red and blue galaxies as described in §3.1. Low-mass galaxies on the  $z = 0$  red sequence, which are predominantly satellites, are quenched at fairly late times (generally  $z < 1$ ). Massive galaxies  $\gtrsim 10^{11} M_{\odot}$  are quenched earlier, typically at  $z \gtrsim 1$  and beyond.

The bottom left panel of Figure 5 shows, as a function of the  $z = 0$  stellar mass, the fractional mass growth of red sequence galaxies between the redshift of quenching and

the present day,  $y \equiv M_{\text{stellar}}(z = 0)/M_{\text{stellar}}(z = z_{\text{quench}})$ . Since many galaxies are quenched at late times, and such galaxies have not had time to undergo mergers, we only plot the mass growth for galaxies with  $z_{\text{quench}} > 0.5$ . This gives a long enough time baseline ( $\sim 5$  Gyr, much longer than the halo dynamical times) to assess red galaxy growth via mergers. Galaxy points are colour-coded by  $z_{\text{quench}}$ , as indicated on the right side of the panel.

Departures from the  $y = 1$  line (i.e. no change in stellar mass, dotted line) increase with quenching redshift: The blue points that are the most recently quenched galaxies typically lie near  $y = 1$ , and in fact are slightly below owing to stellar mass loss. At higher quenching redshifts, galaxies span a wider range in  $y$ . In some cases, galaxies lose mass catastrophically by tidal interactions with other galaxies, and end up near  $y = 0$ . A significant proportion of galaxies quenched at earlier times with  $M > 10^{10.5} M_{\odot}$ , how-

ever, have grown substantially, by factors up to  $\sim 3$ . Since these massive galaxies live in high-density environments, and they've been quenched for longer, they have had more opportunities to acquire mass via mergers than their lower-mass counterparts. Hence  $y$  reflects the amount of mass growth by mergers in massive galaxies since the time of quenching, and in fact underestimates the growth since stellar mass loss also occurs.

To further explore the nature of post-quenching mass growth in our model, we use our merger tree to separate major mergers (those with a mass ratio larger than 1:3) from minor mergers (any merger with a lower mass ratio). We include in the minor merger component accretion of existing stars that live in poorly-resolved galaxies, but this has little impact on the results. The top right panel of Figure 5 shows the fraction of  $z = 0$  red sequence galaxies that have undergone at least one major merger since being quenched. Again, we restrict this analysis to galaxies quenched before  $z = 0.5$ . We also split these galaxies further by quenching redshift into high- (dashed,  $z_{\text{quench}} > 1.5$ ) and low-redshift (dotted,  $0.5 < z_{\text{quench}} < 1.0$ ) bins.

Figure 5 shows that post-quenching major mergers are generally rare, happening in typically only  $\sim 10\%$  of the cases at most masses, with a mild peak up to  $\sim 20\%$  at  $M_* \sim 10^{11} M_\odot$ . Galaxies quenched at the earliest times have major merger fractions as high as 30%. At higher masses we begin to be limited by our simulation volume, as such galaxies become sufficiently rare for mergers between them may be underrepresented. Nevertheless, since many red sequence galaxies have grown by much more than 20% in mass (even while undergoing stellar mass loss), this result immediately suggests that major mergers play a sub-dominant role in the overall growth of massive red galaxies.

With little or no in situ star formation, the growth of these galaxies must therefore owe predominantly to minor mergers. The bottom right panel of Figure 5 shows the mean mass-weighted merger mass ratio as a function of  $z = 0$  stellar mass. By mass-weighting, we can assess the contribution that mergers of a given mass ratio make to the overall growth of passive galaxies. Again we only include galaxies that became red at  $z > 0.5$ , and we also split the sample into high- and low- $z_{\text{quench}}$  sub-samples. The typical merger mass ratio for red sequence galaxies in our simulations is  $\sim 0.2$ , below the commonly-used 1/3 cutoff for major mergers (thin dotted line). Our typical value agrees with that obtained in higher-resolution individual galaxy re-simulations by Oser et al. (2011). Galaxies quenched early on all have roughly the same mean merger mass ratio, whereas galaxies quenched at later times show variation with  $z = 0$  stellar mass such that the most massive and least massive galaxies have higher mass ratios than those in the middle. At all stellar masses, red galaxy mass growth is dominated by minor mergers.

In summary, massive red sequence galaxies in our simulation grow by factors of up to several in mass between the time they are quenched (typically  $z \sim 1$ ) and redshift 0. Lower mass passive galaxies (both satellites and centrals) tend to be quenched at later epochs, and grow less, typically even diminishing in mass owing to stellar evolution. Mass growth at all masses is dominated by minor mergers with a characteristic ratio of 1:5, with at most a 30% contribution from major mergers.

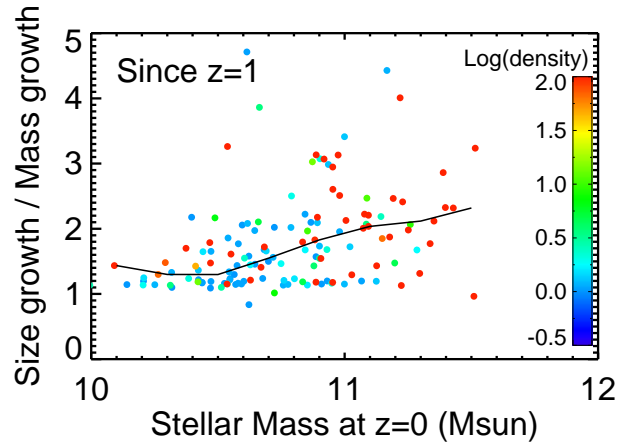


**Figure 6.** The ratio of size growth to mass growth for red sequence galaxies, since  $z = 1$ , as a function of their stellar mass at  $z = 0$ . A solid line indicates the median. Points are colour-coded by the local galaxy density. More massive galaxies, which live in denser environments, show more size growth than lower-mass ones. In some rare cases the galaxy size may evolve several times ( $\sim 3$ ) more than the mass. This is roughly in line with observations, where the ratio is typically  $\sim 2$  for evolution since  $z \sim 2$ .

## 4.2 Size evolution

Observations indicate that massive passive galaxies are more compact at high redshifts than at  $z \sim 0$  by factors of up to 6 or more (Toft et al. 2007; van der Wel et al. 2008; van Dokkum et al. 2008). While observational biases presented an initial concern, recent work suggests that much of the evolution must be physical, and probably arises from a combination of several physical processes. These processes include adiabatic expansion associated with stellar mass loss, major mergers, minor mergers, and evolution in mass-to-light ratios (e.g. Boylan-Kolchin et al. 2006; Naab et al. 2009; Hopkins et al. 2010).

Our simulations make specific predictions about the distribution of merger mass ratios that contribute to red galaxy growth. Therefore, even though the spatial resolution of our simulations is not well-suited to study the internal structure of individual galaxies, we can use simple analytic merger-based estimates to approximate the size growth that our simulated galaxies might undergo.

We construct a simple model for the effects of mergers following the formalism presented in Naab et al. (2009), which arises directly from the virial theorem plus energy conservation. This is appropriate for a purely collisionless system, so we implicitly ignore any (presumably minor) effects of dissipation. Given a stellar accretion event (i.e. a merger) of mass  $M_a$  onto a galaxy of mass  $M_g$ , the ratio of final to initial size of the galaxy is given by:

$$\frac{r_f}{r_i} = \frac{(1 + \eta)^2}{1 + \eta\epsilon}. \quad (1)$$

Here,  $\eta = M_a/M_g$  is the fractional mass increase, and  $\epsilon = \langle v_a^2 \rangle / \langle v_g^2 \rangle$  is the ratio of the two galaxies' stellar populations' mean square velocity dispersions. Using high-resolution simulations, Naab et al. (2009) has shown that

this formula accurately describes the size evolution of early-type galaxies undergoing hierarchical mergers.

To estimate size growth, we must therefore estimate the mass ratio and the velocity dispersion ratio between the satellite (i.e. less massive) and central (more massive) galaxies. We know the ratio of stellar masses directly from our merger tree. For the velocity dispersion, since we cannot accurately resolve it in our simulations, we instead employ an observational result relating it to stellar mass from Gallazzi et al. (2006):  $\log \sigma = -0.895 + 0.286 \log M_{\text{stellar}}$ . With this relation, we obtain  $\epsilon = (\sigma_a/\sigma_g)^2 = (M_a/M_g)^{0.57}$ . Thus, for each merger event, we can calculate the fractional size growth of the remnant galaxy. Taking each  $z = 0$  red galaxy, we consider its entire merger history since being quenched. We account for the size growth of each of its merger events and multiply them to find the galaxy’s total fractional mass growth.

We show the results of this exercise in Figure 6, which shows the size growth relative to mass growth ( $r_f M_i / r_i M_f$ ) as a function of stellar mass. We plot this quantity instead of merely size growth because massive red galaxies in our simulations may not grow the correct amount of stellar mass, as hinted by the number density discrepancies in §3.1. We account for this difficulty by comparing the size growth relative to the mass growth of galaxies, which is a reflection of the prevalence of minor vs. major mergers.

Based on this simple modeling, minor mergers appear to be numerous enough to drive the factors of several in size growth of passive galaxies over time. Galaxies with stellar masses  $> 10^{11} M_\odot$  show typical size growth a factor of 2 greater than their mass growth, indicating that a series of minor mergers tends to puff up these galaxies, as argued by Naab et al. (2009). Lower mass galaxies have not grown as much since moving onto the red sequence, since as we showed in Figure 5 they undergo less merging. These results, using a simple analytic model, are broadly consistent with the idea that minor mergers drive the rapid size growth seen in massive red galaxies since high redshift.

In Figure 6 we also colour-code galaxies by their ( $z = 0$ ) local galaxy densities (which we discuss further in the following section). We note that all galaxies shown are in relatively dense regions compared to blue galaxies. Density is correlated with stellar mass for these passive galaxies (§5.2), so that the galaxies in high-density regions (red points) lie on the right side of the plot. Since size growth (relative to mass growth) appears to increase with stellar mass in Figure 6, galaxies in denser regions tend to undergo more size evolution than those in less-dense regions. At fixed mass  $\sim 10^{11} M_\odot$  there is a weak correlation between size growth and density. This qualitatively agrees with recent observations indicating that galaxies in high-density regions must undergo more evolution in the mass-size relation since  $z = 1$  than their counterparts in lower-density regions (Raichoor et al. 2011). Physically, based on our merger-driven size growth model, this suggests that red galaxies in the densest regions (i.e. galaxy groups in our simulations) tend to undergo a higher proportion of minor mergers.

In summary, a simple model of red galaxy size growth driven by mergers shows that massive galaxies with  $\gtrsim 10^{11} M_\odot$  in our simulation typically have grown in size by a factor of 2 relative to their mass growth since  $z = 1$ . The

degree of size growth increases with stellar mass, and galaxies in denser regions grow by larger factors. These results are broadly consistent with observations as well as previous simulation results.

## 5 ENVIRONMENTAL FACTORS

### 5.1 Bivariate dependence of environment on colour and $M_{\text{stellar}}$

We have shown that the massive and low-mass ends of the red sequence grow first in our model – not until  $z \lesssim 0.3$  do galaxies around  $10^{10} M_\odot$  appear in comparable numbers along the red sequence. Surprisingly, some of these galaxies are identified as central galaxies in a halo that is below the quenching threshold, rather than as satellites within a quenched halo. In this section, we examine how environmental factors drive this behaviour.

We illustrate these environmental effects in Figure 7. On the left we show a colour-mass diagram where the galaxies are colour-coded by their local galaxy density. The resulting trend is clear: the very highest and low-mass red galaxies live in the densest regions, while intermediate-mass passive galaxies ( $M_* \sim 10^{10} - 10^{11} M_\odot$ ) live in lower-density regions. This trend matches that seen in SDSS observations, at least qualitatively (Hogg et al. 2003; Kauffmann et al. 2004; Blanton et al. 2005). Physically, this trend emerges because massive galaxies with  $M_* \gtrsim 10^{10.5} M_\odot$ , once massive enough, can get to the red sequence “on their own” by forming their own hot halos even in (relatively) low-density environments. Massive galaxies that are quenched at early epochs live in the highest overdensities, and thus grow to be the most massive galaxies at  $z = 0$  by accreting other galaxies (see §4). Low-mass ( $\lesssim 10^{10.5} M_\odot$ ) galaxies can typically only be quenched by living in the hot environment of more massive neighbors.

In the right panel of Figure 7 we show only *central* galaxies colour-coded by the distance to the nearest halo with a mass  $> 10^{12} M_\odot$ . This is roughly the halo mass where hot halos will form independently in our simulations. Gray crosses are for galaxies within  $10h^{-1}$  kpc of the centers of massive halos, and coloured points are for central galaxies in lower-mass halos. Note that there are many such galaxies along the red sequence at intermediate masses. We colour-code each point based on the ratio of its distance from the center of the nearest massive halo to that halo’s virial radius.

The first clear difference when looking only at centrals is that there is a deficit of  $M_* \sim 10^{10} M_\odot$  red central galaxies, which as we argued in §3.3 arises because these galaxies are predominantly quenched *satellites* that have grown mostly at late times.

However, there are still a fair number of central galaxies that are along the red sequence at intermediate to low masses. Such galaxies at low mass tend to be fairly close to a quenched halo (i.e. the points are blue), and at least some of the intermediate mass ones as well. This suggests a larger environmental effect – these galaxies are part of super-group structures around higher-mass galaxies, whose hot (albeit unvirialised) gas can be felt beyond the virial radius of member galaxies. Alternatively, these galaxies may have passed within  $R_{\text{vir}}$  of a hot halo on an eccentric orbit

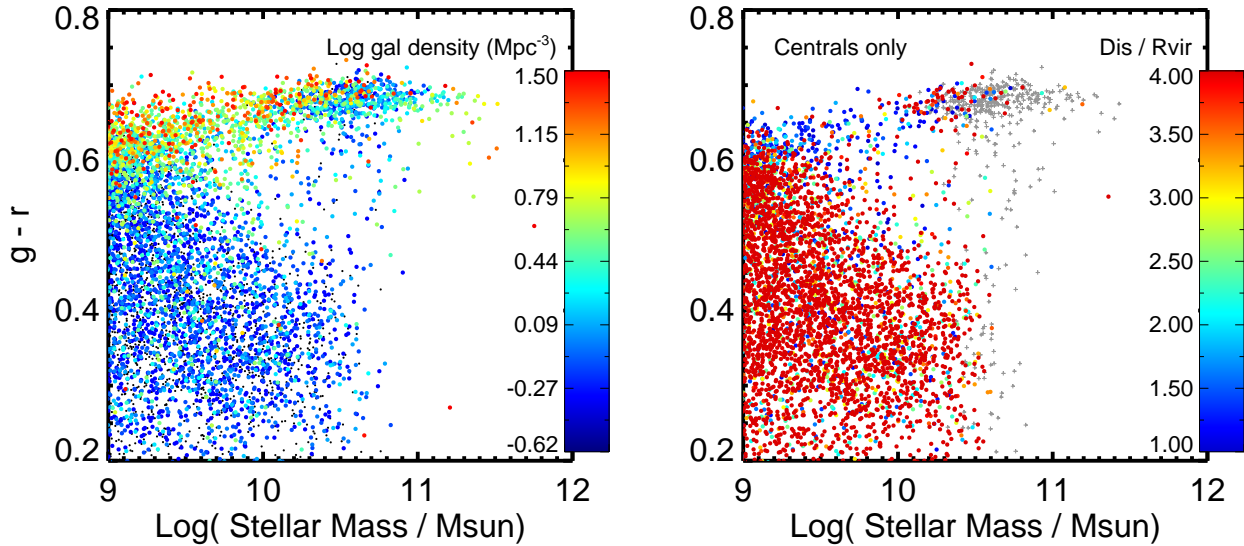


**Figure 7.** **Left** CMD (at  $z = 0$ ) with galaxies colour-coded by the local galaxy density, which is computed by counting the number of galaxies within a radius of 1 Mpc. The high- and low-mass ends of the red sequence live in dense environments, whereas  $\sim L^*$  red sequence galaxies tend to live at lower densities. **Right** Central galaxies are colour-coded by the distance to the closest massive halo (right). Massive halos are defined by a mass of  $10^{12} M_{\odot}$ , as found using a spherical overdensity algorithm. This is roughly the mass at which a halo is dominated by hot gas ( $> 250,000$  K). Grey crosses are galaxies at the centers of their (massive) halos, and blue and red points are outside the virial radius of the nearest massive halo. Some passive galaxies  $< 10^{10.5} M_{\odot}$  are quenched despite living outside  $R_{\text{vir}}$ , suggesting the influence of hot gas in unrelaxed super-group environments. Quenched galaxies at  $\gtrsim 4R_{\text{vir}}$  live in halos just below  $10^{12} M_{\odot}$ , where scatter in the  $M_{\text{halo}}$ –hot gas relation allows them to be hot-gas-dominated.

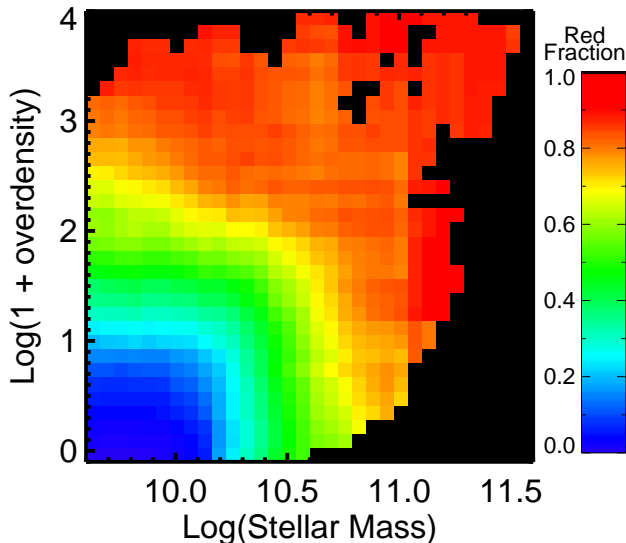


**Figure 8.** Contours of red fraction in stellar mass–overdensity space in our quenching simulation. Galaxies are increasingly red at both higher masses and overdensities. Small galaxies at high overdensity are red because they live within or close to larger halos dominated by hot gas, while larger galaxies are red because they are typically centrals living with hot halos maintained hot via our quenching feedback mechanism.

and been quenched during close passage. This result suggests that environmental factors beyond the halo mass may play some role in quenching of star formation. Observations have

suggested a role for environment (beyond halo mass) in some galaxy properties (Cooper et al. 2008a,b, 2010), though it is typically secondary to galaxy mass.

Figure 8 shows another representation of the relationship between red fraction and environment. Here we plot contours of red fraction (in colors from blue to red) in the plane of stellar mass versus local galaxy overdensity (determined using `Smooth`). This figure can be compared to Figure 6 of Peng et al. (2010), who argued for two different quenching mechanisms, namely “environment quenching” of all galaxies above a given overdensity, and “mass quenching” above a given stellar mass.

Our simulation quantitatively reproduces the observed trends almost exactly, although it has far fewer galaxies than in the SDSS data of Peng et al. (2010), and hence the trends are less smooth and there are regions in this space where this simulation yields no galaxies (black). Broadly, our models reproduce the strong increase in red fraction to both high mass and high overdensity, and the “boxy” contour shape noted by Peng et al. (2010) is indicative of these quenching mechanisms being mostly separable. In our simulations, environment quenching is predominantly associated with satellites at lower masses living in hot halos, although as discussed above there are a fair number of small centrals living in dense environments that are also quenched. Meanwhile, mass quenching is well reproduced by our hot gas threshold for quenching, which translates roughly into a halo mass threshold.

In summary, our simulations are consistent with the interpretation by Peng et al. (2010) that there are two separable quenching mechanisms that deliver galaxies to the red sequence, associated with environment and mass. But our

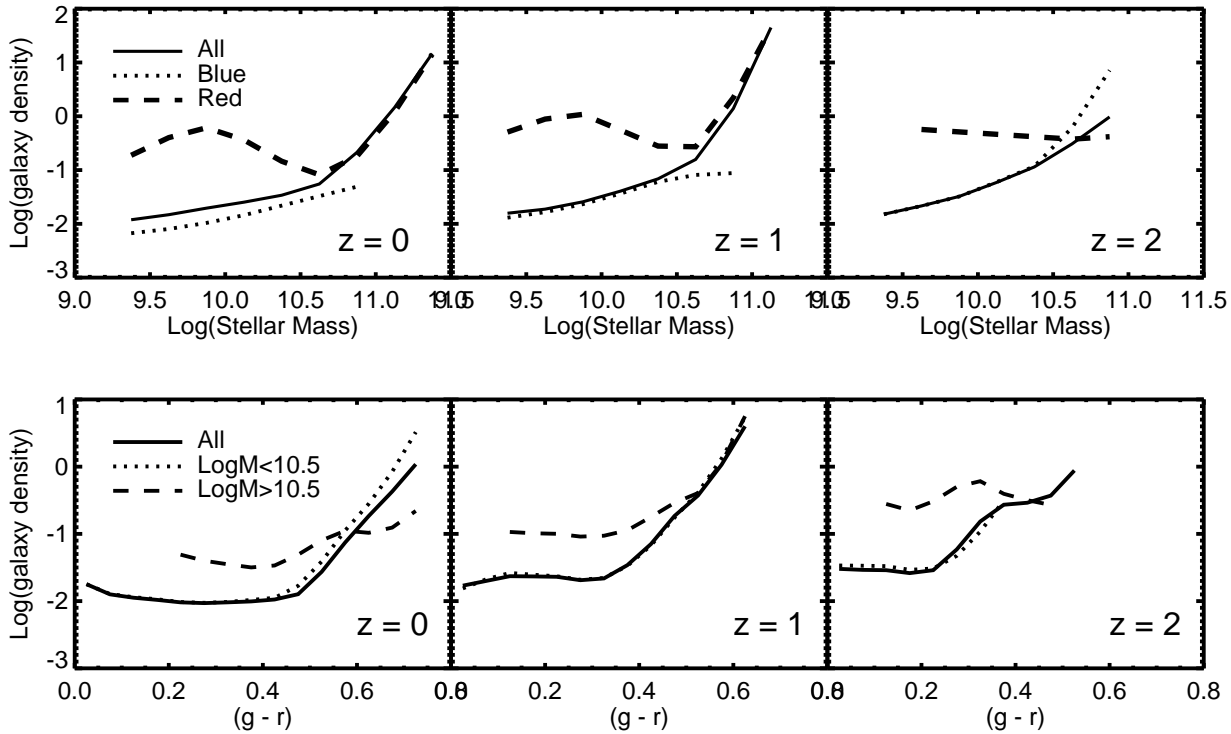


**Figure 9. Top row:** Mass-density relation for all (solid), blue (dotted), and red (dashed) galaxies at  $z = 0, 1$ , and  $2$  (increasing left-to-right). On average (in the “all” sample), galaxies below  $10^{10.5} M_\odot$  consistently live in low density environments, with a sharp rise in local density at higher masses. *Red* galaxies at low masses live in high-density environments, producing a pronounced dip in the red galaxy mass-density relation at  $\sim 10^{10.5} M_\odot$ . Redshift evolution to  $z = 1$  is negligible, and weak at higher  $z$ . **Bottom row:** Colour-density relation for all (solid), low-mass (dotted), and high-mass (dashed) galaxies at three redshifts. On average, blue galaxies live in low-density environments and red galaxies in high-density environments. As expected from the mass-density relation in the top row, massive galaxies tend to live in denser environments than low-mass galaxies, except perhaps for massive *red* galaxies. While the overall colour-evolution of galaxies is apparent in the different panels, the basic trends appear roughly the same at all  $z$ .

simulations further suggest that both mechanisms are ultimately the result of red galaxies living in regions dominated by hot gas, which occurs at both high overdensities and high masses.

## 5.2 Evolution of the mass-density and colour-density relations

We show the evolution of the stellar mass–density relation and the colour–density relation in Figure 9. Here the local galaxy density is found using *Smooth*.

The mass-density relation (top row of Figure 9) for all galaxies shows a very shallow rise in density with mass for stellar masses below  $10^{10.5} M_\odot$ . Above this mass, density rises steeply. This behavior agrees qualitatively with observations at  $z = 0$ , in which a flat slope at low luminosities becomes very steep for the brightest galaxies (Hogg et al. 2003; Blanton et al. 2005). The trends for red and blue galaxies, however, are distinct: Blue galaxies (dotted lines) tend to live in low-density regions and follow the trend for all galaxies at the low-mass end (since they dominate by number). Low-mass and high-mass passive galaxies live in dense regions, while passive galaxies with  $M_* \sim 10^{10} - 10^{11} M_\odot$  live in lower-density regions, as discussed in § 5.1.

For these trends, there is negligible evolution out to

$z = 1$  (top middle panel). Measurements of the  $z = 1$  mass- and colour-density relations have generated some debate in the literature, with recent indications that the colour-density relation persists to  $z \approx 1$  (Cooper et al. 2006, 2007; Elbaz et al. 2007; Scodreggio et al. 2009; Cooper et al. 2010), in accordance with the predicted lack of evolution in Figure 9. At  $z = 2$  (right panel), however, massive blue galaxies live in higher density environments than massive red galaxies. This suggests that the colour-density relation may be inverted for the most massive galaxies at high redshifts in our models. There are two cautionary notes for this, however: first, this result may be sensitive to the division between red and blue galaxies: Figure 1 shows that many blue galaxies are moving toward the red sequence in the  $z = 2$  panel. Second, our quenching criterion may not be capturing the correct physics at these redshifts owing to cold streams penetrating hot halos. Therefore we do not view this high-redshift colour-density inversion as a strong prediction of our models at this time.

The colour-density relation (bottom row of Figure 9) shows similar behavior to the mass-density relation: density is constant for blue colours (low values of  $g-r$ ), then rises steeply for red colours (higher values of  $g-r$ ). When split into high (dashed) and low (dotted) mass galaxies (at  $M_* = 10^{10.5} M_\odot$ ), we see that low-mass galaxies follow the



same trend as for all galaxies. High-mass galaxies, on the other hand, live in higher densities at the blue end, and lower densities at the red end. There are only a handful of blue galaxies with  $M > 10^{10.5} M_\odot$ , and as expected these tend to live in higher density regions than less massive blue galaxies. The fact that the red end of the high-mass curve at  $z = 0$  is at lower densities than most passive galaxies (solid line) is another manifestation of the two-peak shape in the mass-density relation for the red sequence (Figure 7): Red galaxies above  $10^{10.5} M_\odot$  are a mixture of very massive galaxies in high-density regions and  $\sim M^*$  galaxies that are relatively isolated. In contrast, low-mass passive galaxies uniformly reside in high-density regions, since that's the only circumstance under which they become red.

The overall colour-density relation at  $z = 1$  (bottom middle panel) is not significantly different from that at  $z = 0$ . The relation does show some minor evolution for massive galaxies, however. At the red end at  $z = 1$ , high-mass galaxies lie on the overall trend, unlike the  $z = 0$  case where massive red galaxies are in less dense regions. This evolution suggests that many massive galaxies that move onto the red sequence between  $z = 1$  and  $z = 0$  are relatively isolated, and reflects the increasing contribution of intermediate-mass red galaxies with time.

In summary, although our quenching model is most directly tied to hot gas fraction and thus halo mass, environment plays a correlated role in quenching galaxies in our simulations. Since our quenching is directly linked to the proportion of hot gas in a halo and thus halo mass (Birnboim & Dekel 2003; Kereš et al. 2005; Gabor et al. 2011), and halo mass is correlated with environment in a CDM universe, this naturally leads to galaxies in the densest environments being quenched first. Environment plays a key role for a significant fraction of intermediate-mass galaxies that are not in quenched halos themselves but live near quenched halos; these become quenched owing to living in an overdense region pervaded by hot gas beyond the virial radius of massive halos. The latest-arriving members of the red sequence near  $M^*$  typically live in less dense regions, namely isolated halos of  $M \gtrsim 10^{12} M_\odot$ . Evolution in the mass-density and colour-density relations is weak in this model and broadly consistent with data, perhaps showing an inversion in the colour-density relation only at the highest redshifts considered here.

## 6 SUMMARY AND CONCLUSION

We have analysed a cosmological hydrodynamic simulation to explore the evolution of the red sequence. A key feature of our simulation is a simple quenching prescription tied to the dominance of hot gas within the virial radius of a halo. In our quenching prescription, galaxies whose halos have  $> 60\%$  of their baryons in hot gas are starved of star-forming fuel by continual heating of the halo gas. In a previous paper we showed that this simple model yields a distinct red sequence of galaxies whose number densities generally agree with observations (Gabor et al. 2011). This model thus provides a tool for studying the emergence and growth of the red sequence over cosmic time. While some details of our model are overly simplistic and in some cases are in conflict with observations, it serves as representative of a general class of

quenching models where cessation of star formation is driven by the presence of hot coronae or is tied to halo mass.

In our simulations, the first galaxies to turn red at  $z \gtrsim 2$  are among the most massive in the universe at that epoch, with  $M_{\text{stellar}} \sim 10^{10.5-11} M_\odot$ . Satellite galaxies at low masses are concurrently starved of fuel by the same hot halo that triggers our quenching mechanism, and therefore low mass galaxies also appear on the red sequence at early times. Meanwhile, intermediate-mass galaxies at  $\sim 10^{10} - 10^{10.5} M_\odot$  remain predominantly blue until late epochs, producing a pronounced dip in the red galaxy mass function at high redshifts. This dearth of low-mass red galaxies is consistent with observations at moderate ( $\lesssim 1$ ) and high redshift ( $z \gtrsim 2 - 3$ ). At later times, the number of moderate-mass red galaxies catches up to the number of more massive ones, so that the dip in the red galaxy mass function is less pronounced by  $z = 0$ .

Essentially all simulated passive galaxies with stellar mass  $> 10^{11} M_\odot$  form from smaller passive galaxies that grow mass via mergers once on the red sequence. This massive end of the red sequence does not emerge until  $z \sim 1.5$ , and it grows in number by factors of several at late times.

Most of the mass growth of individual passive galaxies is due to minor mergers, with major mergers being rare and a sub-dominant component of mass growth. Based on a simple analytic model, these numerous minor mergers can lead to size growth that is a factor of 2 or more times that of a galaxy's corresponding mass growth. This suggests that minor mergers dominate the dramatic size evolution of massive galaxies, in accordance with earlier work (Naab et al. 2009; Hopkins et al. 2010).

The simple quenching model explored here qualitatively reproduces observed trends among colour, stellar mass, and environment at  $z = 0$ . In detail, it also reproduces the observed mass-density trend for the red sequence: low-mass and high-mass passive galaxies live in the densest regions, whereas galaxies in-between (around  $M^*$ ) live in less dense regions. The mass-density and colour-density trends persist to  $z = 1$ , but the colour-density trend seems to invert for the most massive galaxies at  $z = 2$ . Quenching occurs at both high density, roughly independent of stellar mass, and high stellar mass, roughly independent of density. As argued from corresponding observations by Peng et al. (2010), this indicates two quenching mechanisms associated with environment and mass, which in our model both arise when the local environment is dominated by hot gas.

Our analysis explicitly avoids any considerations of galaxy morphologies. A key question that we therefore do not address is, why are most red and dead galaxies elliptical? While the conventional thinking is that it owes to major mergers that can transform star-forming spirals into elliptical galaxies (Mihos & Hernquist 1996), the simple cessation of star formation at sufficiently early epochs typically results in substantial later growth via dry (i.e. purely or almost purely stellar) mergers. In this scenario, galaxies would quench first when entering a hot halo (or its immediate environment), become red spirals (Bundy et al. 2010), and then undergo subsequent dry mergers that alter its morphology. Our models indicate that larger galaxies living in denser environs undergo more such growth, and so would be expected to have dynamical signatures indicating more dry merging such as boxier isophotes; these trends are qualitatively con-



sistent with observations. Whether the quantitative predictions of this model are in accord with detailed observations remains to be seen.

More broadly, it appears that a quenching mechanism based on a simple hot gas fraction threshold (which is well-correlated with a halo mass threshold) is capable of reproducing a variety of observations not only at the present epoch but also out to  $z \sim 1$  and beyond. However, there are significant failures, such as a dearth of the most massive galaxies, and a too-sharp cutoff in the blue galaxy mass function suggesting that both today and at high redshifts in the real Universe, some galaxies are able to be star-forming despite living in hot gas-dominated halos. Hence this model represents only a step towards understanding the physical processes driving red galaxy evolution. Comparisons to observations particularly probing the intermediate-mass regime out to high redshifts can place strong constraints on models such as these, and highlight additional physical processes that may need to be considered.

## REFERENCES

- Abadi M. G., Moore B., Bower R. G., 1999, *MNRAS*, 308, 947
- Agertz O. et al., 2007, *MNRAS*, 380, 963
- Baldry I. K., Glazebrook K., Driver S. P., 2008, *MNRAS*, 388, 945
- Barnes J. E., 1990, *Nature*, 344, 379
- Beckwith S. V. W. et al., 2006, *AJ*, 132, 1729
- Bekki K., Couch W. J., Shioya Y., 2002, *ApJ*, 577, 651
- Bell E. F., McIntosh D. H., Katz N., Weinberg M. D., 2003, *ApJS*, 149, 289
- Bell E. F. et al., 2004, *ApJ*, 608, 752
- Berlind A. A. et al., 2003, *ApJ*, 593, 1
- Binney J., 1977, *ApJ*, 215, 483
- Birnboim Y., Dekel A., 2003, *MNRAS*, 345, 349
- Birnboim Y., Dekel A., Neistein E., 2007, *MNRAS*, 380, 339
- Blanton M. R., 2006, *ApJ*, 648, 268
- Blanton M. R., Eisenstein D., Hogg D. W., Schlegel D. J., Brinkmann J., 2005, *ApJ*, 629, 143
- Bower R. G., Benson A. J., Malbon R., Helly J. C., Frenk C. S., Baugh C. M., Cole S., Lacey C. G., 2006, *MNRAS*, 370, 645
- Bower R. G., Kodama T., Terlevich A., 1998, *MNRAS*, 299, 1193
- Boylan-Kolchin M., Ma C.-P., Quataert E., 2006, *MNRAS*, 369, 1081
- Brammer G. B. et al., 2011, *ApJ*, 739, 24
- Brammer G. B. et al., 2009, *ApJ*, 706, L173
- Brown M. J. I., Dey A., Jannuzi B. T., Brand K., Benson A. J., Brodwin M., Croton D. J., Eisenhardt P. R., 2007, *ApJ*, 654, 858
- Bruzual G., Charlot S., 2003, *MNRAS*, 344, 1000
- Bundy K. et al., 2010, *ApJ*, 719, 1969
- Cattaneo A., Dekel A., Devriendt J., Guiderdoni B., Blaizot J., 2006, *MNRAS*, 370, 1651
- Chabrier G., 2003, *ApJ*, 586, L133
- Cool R. J. et al., 2008, *ApJ*, 682, 919
- Cooper M. C. et al., 2010, *MNRAS*, 409, 337
- Cooper M. C. et al., 2007, *MNRAS*, 376, 1445
- Cooper M. C. et al., 2006, *MNRAS*, 370, 198
- Cooper M. C., Newman J. A., Weiner B. J., Yan R., Willmer C. N. A., Bundy K., Coil A. L., Conselice C. J., Davis M., Faber S. M., Gerke B. F., Guhathakurta P., Koo D. C., Noeske K. G., 2008a, *MNRAS*, 383, 1058
- Cooper M. C., Tremonti C. A., Newman J. A., Zabludoff A. I., 2008b, *MNRAS*, 390, 245
- Cox T. J., Dutta S. N., Di Matteo T., Hernquist L., Hopkins P. F., Robertson B., Springel V., 2006, *ApJ*, 650, 791
- Croton D. J. et al., 2006, *MNRAS*, 365, 11
- Daddi E. et al., 2007, *ApJ*, 670, 156
- Daddi E. et al., 2005, *ApJ*, 626, 680
- Davé R., 2008, *MNRAS*, 385, 147
- Davé R., Finlator K., Oppenheimer B. D., 2006, *MNRAS*, 370, 273
- , 2007, in *EAS Publications Series*, Vol. 24, *EAS Publications Series*, E. Emsellem, H. Wozniak, G. Massacrier, J.-F. Gonzalez, J. Devriendt, & N. Champavert, ed., pp. 183–189
- , 2011a, *MNRAS*, 416, 1354
- Davé R., Oppenheimer B. D., Finlator K., 2011b, *MNRAS*, 415, 11
- Davé R., Oppenheimer B. D., Sivanandam S., 2008, *MNRAS*, 391, 110
- De Lucia G., Fontanot F., Wilman D., Monaco P., 2011, *MNRAS*, 414, 1439
- Dekel A., Birnboim Y., 2006, *MNRAS*, 368, 2
- Dekel A., Sari R., Ceverino D., 2009, *ApJ*, 703, 785
- Di Matteo T., Springel V., Hernquist L., 2005, *Nature*, 433, 604
- Drory N. et al., 2009, *ApJ*, 707, 1595
- Elbaz D. et al., 2007, *A&A*, 468, 33
- Faber S. M. et al., 2007, *ApJ*, 665, 265
- Finlator K., Davé R., 2008, *MNRAS*, 385, 2181
- Finlator K., Davé R., Oppenheimer B. D., 2007, *MNRAS*, 376, 1861
- Finlator K., Davé R., Papovich C., Hernquist L., 2006, *ApJ*, 639, 672
- Gabor J. M., Davé R., Finlator K., Oppenheimer B. D., 2010, *MNRAS*, 407, 749
- , 2011, *MNRAS*, 407, 749
- Gallagher III J. S., Ostriker J. P., 1972, *AJ*, 77, 288
- Gallazzi A., Charlot S., Brinchmann J., White S. D. M., 2006, *MNRAS*, 370, 1106
- Gelb J. M., Bertschinger E., 1994, *ApJ*, 436, 467
- Grogin N. A. et al., 2011, *ArXiv e-prints*
- Gunn J. E., Gott J. R. I., 1972, *ApJ*, 176, 1
- Haardt F., Madau P., 2001, in *Clusters of Galaxies and the High Redshift Universe Observed in X-rays*, D. M. Neumann & J. T. V. Tran, ed.
- Hogg D. W. et al., 2002, *AJ*, 124, 646
- Hogg D. W. et al., 2003, *ApJ*, 585, L5
- Hopkins P. F., Bundy K., Hernquist L., Wuyts S. and Cox T. J., 2010, *MNRAS*, 401, 1099
- Hopkins P. F., Cox T. J., Kereš D., Hernquist L., 2008, *ApJS*, 175, 390
- Hopkins P. F., Hernquist L., Cox T. J., Robertson B., Springel V., 2006, *ApJS*, 163, 50
- Jungwiert B., Combes F., Palouš J., 2001, *A&A*, 376, 85
- Kauffmann G., White S. D. M., Heckman T. M., Ménard B., Brinchmann J., Charlot S., Tremonti C., Brinkmann J., 2004, *MNRAS*, 353, 713

- Kennicutt Jr. R. C., 1998, *ApJ*, 498, 541
- Kereš D., Katz N., Fardal M., Davé R., Weinberg D. H., 2009, *MNRAS*, 395, 160
- Kereš D., Katz N., Weinberg D. H., Davé R., 2005, *MNRAS*, 363, 2
- Koekemoer A. M. et al., 2011, *ArXiv e-prints*
- Komatsu E. et al., 2009, *ApJS*, 180, 330
- Kriek M., van der Wel A., van Dokkum P. G., Franx M., Illingworth G. D., 2008, *ApJ*, 682, 896
- Larson R. B., Tinsley B. M., Caldwell C. N., 1980, *ApJ*, 237, 692
- Maller A. H., Katz N., Kereš D., Davé R., Weinberg D. H., 2006, *ApJ*, 647, 763
- Marchesini D. et al., 2010, *ApJ*, 725, 1277
- Martin C. L., 2005, *ApJ*, 621, 227
- McKee C. F., Ostriker J. P., 1977, *ApJ*, 218, 148
- Mihos J. C., Hernquist L., 1996, *ApJ*, 464, 641
- Moore B., Lake G., Katz N., 1998, *ApJ*, 495, 139
- Murante G. et al., 2004, *ApJ*, 607, L83
- Murray N., Quataert E., Thompson T. A., 2005, *ApJ*, 618, 569
- Naab T., Johansson P. H., Ostriker J. P., 2009, *ApJ*, 699, L178
- Oppenheimer B. D., Davé R., 2006, *MNRAS*, 373, 1265
- , 2008, *MNRAS*, 387, 577
- Oppenheimer B. D., Davé R., Kereš D., Fardal M., Katz N., Kollmeier J. A., Weinberg D. H., 2010, *MNRAS*, 406, 2325
- Oser L., Naab T., Ostriker J. P., Johansson P. H., 2011, *ArXiv e-prints*
- Peng Y.-j. et al., 2010, *ApJ*, 721, 193
- Quilis V., Moore B., Bower R., 2000, *Science*, 288, 1617
- Raichoor A. et al., 2011, *ArXiv e-prints*
- Rees M. J., Ostriker J. P., 1977, *MNRAS*, 179, 541
- Richstone D. O., 1976, *ApJ*, 204, 642
- Rudnick G. et al., 2009, *ApJ*, 700, 1559
- Rupke D. S., Veilleux S., Sanders D. B., 2005, *ApJS*, 160, 115
- Salim S. et al., 2007, *ApJS*, 173, 267
- Scannapieco E., Pichon C., Aracil B., Petitjean P., Thacker R. J., Pogosyan D., Bergeron J., Couchman H. M. P., 2006, *MNRAS*, 365, 615
- Scodeggio M. et al., 2009, *A&A*, 501, 21
- Sijacki D., Springel V., Di Matteo T., Hernquist L., 2007, *MNRAS*, 380, 877
- Silk J., 1977, *ApJ*, 211, 638
- Simha V., Weinberg D. H., Davé R., Gnedin O. Y., Katz N., Kereš D., 2009, *MNRAS*, 399, 650
- Somerville R. S., Hopkins P. F., Cox T. J., Robertson B. E., Hernquist L., 2008, *MNRAS*, 391, 481
- Somerville R. S., Primack J. R., Faber S. M., 2001, *MNRAS*, 320, 504
- Springel V., 2005, *MNRAS*, 364, 1105
- Springel V., Di Matteo T., Hernquist L., 2005, *ApJ*, 620, L79
- Springel V., Hernquist L., 2003, *MNRAS*, 339, 289
- Steidel C. C., Erb D. K., Shapley A. E., Pettini M., Reddy N., Bogosavljević M., Rudie G. C., Rakic O., 2010, *ApJ*, 717, 289
- Stutz A. M., Papovich C., Eisenstein D. J., 2008, *ApJ*, 677, 828
- Sutherland R. S., Dopita M. A., 1993, *ApJS*, 88, 253
- Taylor E. N. et al., 2009, *ApJ*, 694, 1171
- Toft S. et al., 2007, *ApJ*, 671, 285
- Toft S., van Dokkum P., Franx M., Thompson R. I., Illingworth G. D., Bouwens R. J., Kriek M., 2005, *ApJ*, 624, L9
- Trager S. C., Faber S. M., Dressler A., 2008, *MNRAS*, 386, 715
- Trager S. C., Worthey G., Faber S. M., Burstein D., Gonzalez J. J., 1998, *ApJS*, 116, 1
- van der Wel A., Bell E. F., Holden B. P., Skibba R. A., Rix H.-W., 2010, *ApJ*, 714, 1779
- van der Wel A., Holden B. P., Zirm A. W., Franx M., Retura A., Illingworth G. D., Ford H. C., 2008, *ApJ*, 688, 48
- van Dokkum P. G. et al., 2008, *ApJ*, 677, L5
- van Dokkum P. G. et al., 2010, *ApJ*, 709, 1018
- Wang B., Heckman T. M., 1996, *ApJ*, 457, 645
- Whitaker K. E. et al., 2010, *ApJ*, 719, 1715
- White S. D. M., Frenk C. S., 1991, *ApJ*, 379, 52
- White S. D. M., Rees M. J., 1978, *MNRAS*, 183, 341